Journal of Materials Chemistry A

A facile method for the synthesis of a porous cobalt oxide-carbon hybrid as a highly efficient water oxidation catalyst

Journal:	*Journal of Materials Chemistry A*
Manuscript ID	TA-ART-09-2015-007813.R1
Article Type:	Paper
Date Submitted by the Author:	22-Dec-2015

Complete List of Authors:	Zhang, Mei; Sun Yat-Sen University, School of Chemistry and Chemical Engineering; School of Chemistry & Chemical, inorganic chemistry Huang, Yong-Liang; Sun Yat-Sen University, School of Chemistry and Chemical Engineering, Wang, Jia-Wei; Sun Yat-Sen University, School of Chemistry and Chemical Engineering Lu, Tong-Bu; Sun Yat-Sen University, School of Chemistry and Chemical Engineering

Journal of Materials Chemistry A RSC Publishing

PAPER

A facile method for the synthesis of a porous cobalt oxide-carbon hybrid as a highly efficient water oxidation catalyst

Cite this: DOI: 10.1039/x0xx00000x

Received ooth,
Accepted ooth

DOI: 10.1039/x0xx00000x

www.rsc.org/

Mei Zhang, Yong-Liang Huang, Jia-Wei Wang and Tong-Bu Lu*

A main challenge for light-driven water splitting is the development of efficient and economical water oxidation catalysts (WOCs). Herein, we developed a facile approach for the preparation of a porous cobalt oxide-carbon hybrid, which was prepared by carbonizing in the inert atmosphere and subsequently air-calcining nanocrystals of zeolite imidazole framework-67 (ZIF-67), and utilized as an efficient WOC. Using $Ru(bpy)_3(PF_6)_3$ as an oxidant, we got a record catalytic turnover number (TON) and turnover frequency (TOF) of 910 ± 21 and 14.6 ± 0.4 s^{-1} per cobalt atom, respectively. In addition, the synthesized catalyst can also act as an efficient electrochemical WOC, with a low OER overpotential of 0.36 V at 10.0 mA cm^{-2} in pH 13 medium. The superior catalyst's performance can be attributed the homogeneous dispersion of CoO_x and in situ formed porous carbon, and the presence of nitrogen in the catalyst may also attribute to its high catalytic activity.

Introduction

Water oxidation is regarded as the bottleneck in water splitting for renewable solar fuel production (such as H_2 and hydrocarbons), as it is a slow kinetics of the reaction and requires a high overpotential to achieve a complex four-electron oxidation process.[1] Despite the enormous chemical challenge, visible-light driven water oxidation is essential because it is the only way we can obtain sufficient waste-free electrons economically for the solar fuel production on a terawatt scale to supply our energy demands.[1e,1f] In deed, photochemical water oxidation takes place in photosystem II (PSII) in green plants, in which Mn_4O_4Ca serves as a chemical WOC. Although some noble metal oxides such as IrO_2 and RuO_2 show a high catalytic efficiency for oxygen evolution reaction (OER), their high cost restricts their use on a large scale.[2] The development of efficient and economical water oxidation catalysts (WOCs) is one of the main challenges of current research in renewable energies.[3]

Recently, WOCs based on first row transition metal oxides and their derivatives are attractive due to their economy and stability.[4,5] Among them, cobalt oxides-based WOCs,[5] especially Co_3O_4,[5g-5n] have been investigated extensively, as they have shown high OER activity both as electrochemical and photochemical WOCs. Usually, a catalyst with a smaller particle exhibits a higher catalytic activity, as smaller particle has more cobalt atoms sitting on the particle surface to act as catalytic centers for oxygen evolution. However, the smaller nanoparticles make them easier to aggregate. An efficient approach to avoid the small nanoparticle aggregation is carbonization of metal-organic frameworks (MOFs) to produce porous metal oxide-carbon hybrid,[5j,6] as the periodic arrangement of metal ions and organic motifs in the frameworks of MOFs leads to a homogeneous distribution of metal oxide nanoparticles and in situ formed carbon species.[5j,6a-6b] As zeolite imidazole framework-67 (ZIF-67) is easy to prepare and economical,[7] many groups used ZIF-67 as a precursor to prepare porous carbon and metal oxides-carbon hybrids as catalysts for the oxygen reduction reaction (ORR),[8] and more recently, Chen et al used ZIF-67 and graphene oxide as precursors for the preparation of nitrogen-doped graphene/cobalt-embedded porous carbon as electrochemical WOC.[8b] However, it has not reported using ZIF-67 as a precursor for the preparation of porous cobalt oxide-carbon hybrid as a chemical WOC.

For practical use on a large scale, we should obtain a WOC with both high catalytic efficiency and economy, thus it is important to develop facile methods for the synthesis of WOCs to reduce their price. Given its easy to prepare and economical, as well as the high cobalt content and good framework stability, ZIF-67 was chosen as

MOE Key Laboratory of Bioinorganic and Synthetic Chemistry, School of Chemistry and Chemical Engineering, Sun Yat-Sen University, Guangzhou 510275 (China)
Fax: (+86)20-8411-2921; E-mail: lutongbu@mail.sysu.edu.cn

† Electronic supplementary information (ESI) available: SEM, TEM and HRTEM images; PXRD and XPS patterns; Tables; Oxygen evolution curves. See DOI: 10.1039/b000000x/

an ideal precursor for the preparation of porous cobalt oxide-carbon hybrid as a WOC. Furthermore, as smaller crystal sizes will lead to a larger surface area, nanocrystals of ZIF-67 were prepared according to the reported method (Figure S1).[9] Therefore, we performed an *in situ* calcination on a nanocrystalline ZIF-67 under different temperatures to get a series of porous CoO_x-carbon hybrids (Figure 1), and their chemical and photochemical OER activities were investigated. Under the optimized conditions, CoO_x-carbon hybrid carbonized at 700 °C displays the highest OER activity under near neutral medium (pH = 8.5), with record TOFs of 14.6 and 0.039 s^{-1} per cobalt atom under chemical and photochemical water oxidation conditions, respectively.

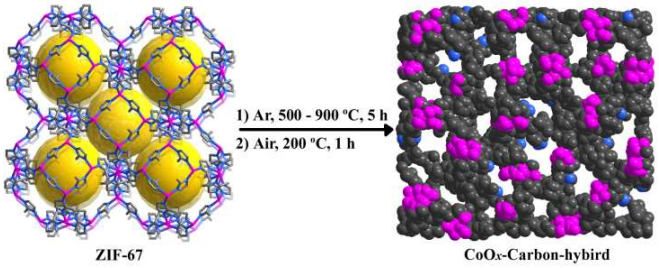

Fig 1. Schematic representation of the formation of CoO_x-carbon hybrids through the two-step thermal treatment of ZIF-67 (grey, blue and magenta spheres represent C, N and CoO_x in the hybrid, respectively).

Experimental

General procedures and materials.

Unless otherwise noted, materials were obtained from commercial suppliers and were used without further purification. Scanning electron microscopy (SEM) images were collected by field emission scanning electron microscope (FEI, Quanta 400). Transmission electron microscopy images (TEM), energy dispersive X-ray spectroscopy (EDS) and high resolution transmission electron microscopy (HRTEM) were collected by JEM2010-HR (200 kV). EDS elemental mapping images were conducted by FEI Tecnai G2 F30 (300 kV). Elemental analyses were determined using an Elementar Vario EL elemental analyzer. Co ion contents were determined by a TJA IRIS (HR) inductively coupled plasma-atomic emission spectrometer (ICP). The powder X-ray diffraction measurements were performed on a D8 ADVANCE X-ray Diffractometer. Gas sorption was measured with a BELSORP-max gas adsorption instrument. The N_2 adsorption isotherms were collected in a relative pressure range from 10^{-4} to 1 atm. The cryogenic temperature of 77 K required for N_2 sorption tests was controlled using liquid nitrogen bath. The initial outgassing process for the sample was carried out under a high vacuum (less than 10^{-6} mbar) at 120 ºC for 6 h. The desolvated sample and sample tube were weighed precisely and transferred to the analyzer. Thermogravimetric (TG) analysis data were collected on a Netzsch TG-209 instrument under a nitrogen atmosphere in the temperature range 20−1000 °C, with a heating rate of 10 °C min^{-1}. The XPS data were collected on an ESCA Lab250 instrument. The production of oxygen was recorded in liquid phase by a Clark-type oxygen electrode (Hansatech, Oxygraph system).

The preparation of nano zeolite imidazole framework-67 (ZIF-67).[9]

A methanol solution (200 mL) of $Co(NO_3)_2{\cdot}6H_2O$ (6.57 g, 80 mmol) was poured into a methanol solution (200 mL) of 2-methyl-1H-imidazole (2.91 g, 10 mmol) under stirring. The mixture was stirred at room temperature for 30 min, the nanocrystals of ZIF-67 were isolated by centrifugation, washed with ethanol and dried under 80 °C (Figure S1). Yield: 1.40 g, 63%.

The preparation of nano Co_3O_4 (ZIF-67-Co_3O_4).

The as-synthesized nano-ZIF-67 was firstly heated from room temperature to corresponding carbonization temperature (500 °C) under argon with a heating rate of 10 °C/min, and maintained at this temperature for 5 h. Subsequently, the temperature was decreased to 380 °C and the atmosphere was changed to air and remained at this temperature for 5 h to get the product of ZIF-67-Co_3O_4.

The preparations of 500-, 600-, 700-, 800- and 900-CoO_x-C.

The as-synthesized nano-ZIF-67 was firstly heated from room temperature to corresponding carbonization temperature (500-900 °C) under argon with a heating rate of 10 °C/min, and maintained at this temperature for 5 h. Subsequently, the temperature was decreased to 200 °C and the atmosphere was changed to air and remained at this temperature for 1 h to get the product of T-CoO_x-C. The results of elemental analyses for T-CoO_x-C are given in Table 1. From Table 1 it can be found that the C contents increase along with the increasing carbonization temperature, while the H and N contents decrease along with the increasing carbonization temperature, and the Co content is the lowest for 700-CoO_x-C. The reason that the sum of elements is not 100% is due to the existence of O element in T-CoO_x-C (see Figure 2d).

Table 1. The results of elemental analyses for T-CoO_x-C

	C (%)	H (%)	N (%)	Co (%)
500-CoO_x-C	27.0	1.8	8.6	49.3
600-CoO_x-C	28.7	1.3	5.6	42.6
700-CoO_x-C	39.9	1.2	3.9	37.5
800-CoO_x-C	43.4	1.0	2.1	40.3
900-CoO_x-C	45.5	0.7	1.1	40.8

Chemical water oxidation.

The concentration of oxygen evolution was measured by a Clark oxygen electrode using $Ru(bpy)_3(PF_6)_3$ as an oxidant. In a typical reaction, a certain amount of $Ru(bpy)_3(PF_6)_3$ and 1.0 mL of water were placed in the Clark oxygen electrode system (2.5 mL), and bubbled with nitrogen for about 2 min to remove dissolved oxygen. After that, the system was maintained for an additional 5 min to record a baseline to guarantee no oxygen leakage or side reaction. About 0.1 mg of catalyst (weighted by a balance with 0.001 mg scale) was homogeneously dispersed in 1.0 mL of water through ultrasonic beforehand for over half hour to get a homogeneous suspension, then a certain amount of aqueous solution of catalyst (for instance, 1 μL for ~0.1 μg) and NaB_i buffer (degassed with nitrogen before use)

were injected into the system to ensure the overall volume of 2 mL. The temperature of the reaction system was kept at 25 °C with a water bath. The TOFs were calculated using the total amount of oxygen generated within initial 20 s. Each experiment was repeated three times to ensure the accuracy and reproducibility of the results.

Photochemical water oxidation.

700-CoO_x-C (0.5 mg) was dispersed in NaPi aqueous buffer (0.5 mL) with a pH value of 8.5 by sonication for 10 min prior to photocatalysis. In a typical experiment, 10 mg of $Ru(bpy)_3(ClO_4)_2$ (4.2 mM), 50 mg of $Na_2S_2O_8$ (68 mM) and 0.1 mg catalyst solution (0.1 mL after ultrasonic dispersion, the concentration of Co is 3.0 μM) were mixed in 3.0 mL buffer in a 5 mL round bottle flask (total volume 9.2 mL) sealed with a rubber stopper, followed by bubbling with Ar gas for 15 min. After that, the round bottle flask was exposed to a 100 W Xe lamp with a 420 nm cut off filter at room temperature. The light intensity of Xe lamp is 320 mW/cm^2 measured by an optical power meter (Newport, 843-R). Additionally, blank control experiment (without catalyst or photosensitizer) was performed under the same condition. The generated oxygen during the water oxidation reaction in the headspace (200 μL) was sampled by a syringe and analyzed by an Agilent 7820A GC system equipped with thermal conductivity detector and a GC column (2 mm) packed with 5Å molecular sieves. Argon was used as a carrier gas.

Stability of 700-CoO_x-C.

After the first run of the photochemical reaction, 700-CoO_x-C was collected by a magnet. A fresh buffer solution containing $Na_2S_2O_8$ (68 mM) and $[Ru(bpy)_3](ClO_4)_2$ (4.2 mM) was added to the collected particles for the repetitive examination. The same method applies to the third cycle.

Electrochemical water oxidation.

Electrochemical water oxidation was studied with a standard three-electrode system controlled by a CHI620E electrochemical workstation. An Ag/AgCl (in 3 M KCl solution) electrode and a platinum electrode were used as the reference electrode and counter electrode, respectively. To prepare the working electrode, 3.925 mg of catalyst and 8 μL of Nafion solution (5 wt %) were dispersed in 0.5 mL of isopropanol−water mixed solvent with a volume ratio of 1:1 with sonication for at least 30 min to generate a homogeneous suspension. Then 5 μL of this solution was drop-casted onto a 5 mm diameter glassy-carbon electrode and then the solvent was evaporated at room temperature overnight, yielding a catalyst loading of 0.2 mg cm^{-2}. Electrochemical impedance spectrum (EIS) measurements were carried out at an applied potential of 1.63 V (*vs.* RHE) in 0.1 M KOH solution on a CHI660E electrochemical workstation (CH Instrument Co.) with an AC amplitude of 5 mV. The impedance spectra were recorded in the frequency range 100 kHz to 0.1 Hz. The experimental impedance data were fitted to a specific equivalent circuit using ZSimPWin software to derive the resistance of the electrodes.

Results and discussion

The result of thermogravimetric analysis (TGA) of ZIF-67 under an inert atmosphere indicates that it begins to decompose at 470 °C and thoroughly decomposes over 1000 °C (Figure S2). Within its thermal decomposition range, nanocrystalline ZIF-67 was firstly carbonized under an argon atmosphere for 5 h at 500, 600, 700, 800 and 900 °C, respectively, and then further calcined in air at 200 °C for 1 h. The obtained CoO_x-carbon hybrid materials are denoted as T-CoO_x-C (where T is the carbonization temperature). Scanning electron microscopy (SEM) images of the synthesized T-CoO_x-C materials are shown in Figure 2, and their characterization is summarized in Table 2. Figure 2a shows the homogenous sizes of ZIF-67 nanocrystalline particles with diameters of ~350 nm. After carbonization and calcination, 700-CoO_x-C retained their homogenous sizes (Figure 2d) with a contracted cubic shape compared to those of nanocrystalline ZIF-67, while 800-CoO_x-C is partly aggregate (Figure 2e), and the morphologies of 500-, 600-, and 900-CoO_x-C became partly or mainly amorphous and only a few of them remained cubic in shape (see Table 2 and Figure 2b, 2c and 2f, respectively). These results indicate that 700°C is the optimal temperature for carbonization of ZIF-67 nanocrystals.

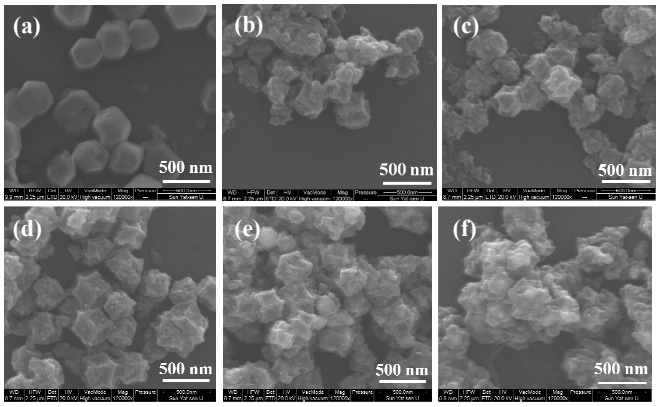

Fig 2. SEM images for (a) ZIF-67 nanocrystals, (b) 500-CoO_x-C, (c) 600-CoO_x-C, (d) 700-CoO_x-C, (e) 800-CoO_x-C, and (f) 900-CoO_x-C.

Table 2. The characterization of the obtained catalysts.

	size (nm)	shape	surface area ($m^2 \cdot g^{-1}$)	crystallinity
ZIF-67	~ 350	cubic		high
500-CoO_x-C	~ 250	mainly amorphous	84	poor
600-CoO_x-C	~ 310	partly amorphous	157	poor
700-CoO_x-C	~ 260	cubic	223	high
800-CoO_x-C	~ 240	cubic with partly aggregate	262	moderate
900-CoO_x-C	~ 310	mainly aggregate	225	poor

According to the powder X-ray diffraction (PXRD) results (Figure 3), the cobalt species in the obtained materials exhibit different forms. The PXRD patterns of the 500- and 600-CoO_x-C samples exhibit peaks that arise from Co_3O_4 and CoO. When

the temperature was increased to 700, 800 and 900 °C, Co_3O_4, CoO and Co coexisted in the 700-, 800- and 900-CoO_x-C samples, respectively. The broad peaks in the range of 20-30° (2θ) in the PXRD patterns of 700-, 800- and 900-CoO_x-C are attributed to the ordered amorphous carbon species that are formed during the carbonization process.[5j] The absence of peaks in the 20-30° (2θ) range of the PXRD patterns of 500- and 600-CoO_x-C indicates that the carbonization temperature was too low to form the ordered amorphous carbon species. The X-ray photoelectron spectroscopy (XPS) results indicate that the binding energies of the Co $2p_{3/2}$ and Co $2p_{1/2}$ peaks are located at 780.7 and 795.8 eV, respectively (Figure 4a). These values are in good accordance with the corresponding values of Co_3O_4,[8e] suggesting that Co_3O_4 is the primary product on the surface of these materials. In comparison to the XPS peak at 780.1 eV in the Co $2p_{3/2}$ spectrum of pure Co_3O_4,[5j] the shift of the corresponding peak at 780.7 eV in the spectrum 700-CoO_x-C indicates the close assembly and strong interaction between Co_3O_4 and carbon.[5j] The presence of Co_3O_4 can be further confirmed by the binding energies of the O 1s peaks observed at 530.0 eV for O_I and 531.6 eV for O_{II} in Co_3O_4 phase[8e,8f] (Figure 4b). Furthermore, the binding energies for C 1s located at 284.7 eV can also be observed (Figure 4c).[8f] With increasing the carbonation temperature, the C contents increase, while the O contents decrease (Figures 4b and 4c), which is consistent with the elemental analyses results.

The specific surface areas of the hybrid materials were measured using N_2 adsorption-desorption analysis (Figure S3) via the Brunauer-Emmett-Teller (BET) method, resulting in the values of 84, 157, 223, 262 and 225 $m^2\ g^{-1}$ for 500-, 600-, 700-, 800- and 900-CoO_x-C, respectively (Tables 1 and S1). Thus, the surface areas of 700-, 800- and 900-CoO_x-C are larger than those of 500- and 600-CoO_x-C. The large surface area of the catalysts is beneficial for the dispersion and utilization of the active sites, which can significantly improve their catalytic efficiency.[10] In addition, the interior structures of the obtained materials were investigated by transmission electron microscopy (TEM) (Figure S4). Figures S4a and S4b show the irregular morphology of CoO_x dispersed in amorphous 500- and

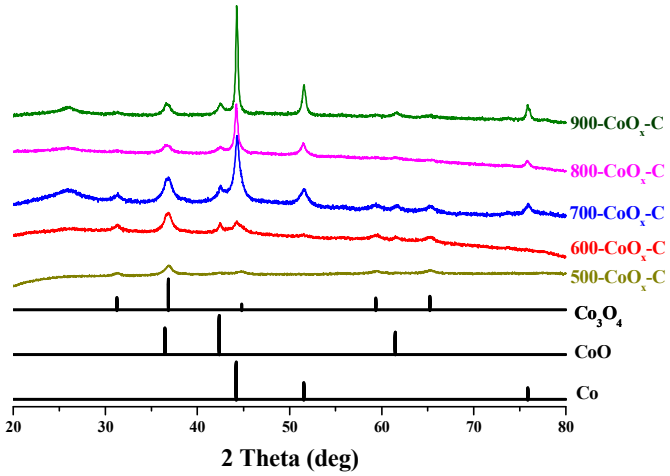

Fig 3. The PXRD patterns for T-CoO_x-C.

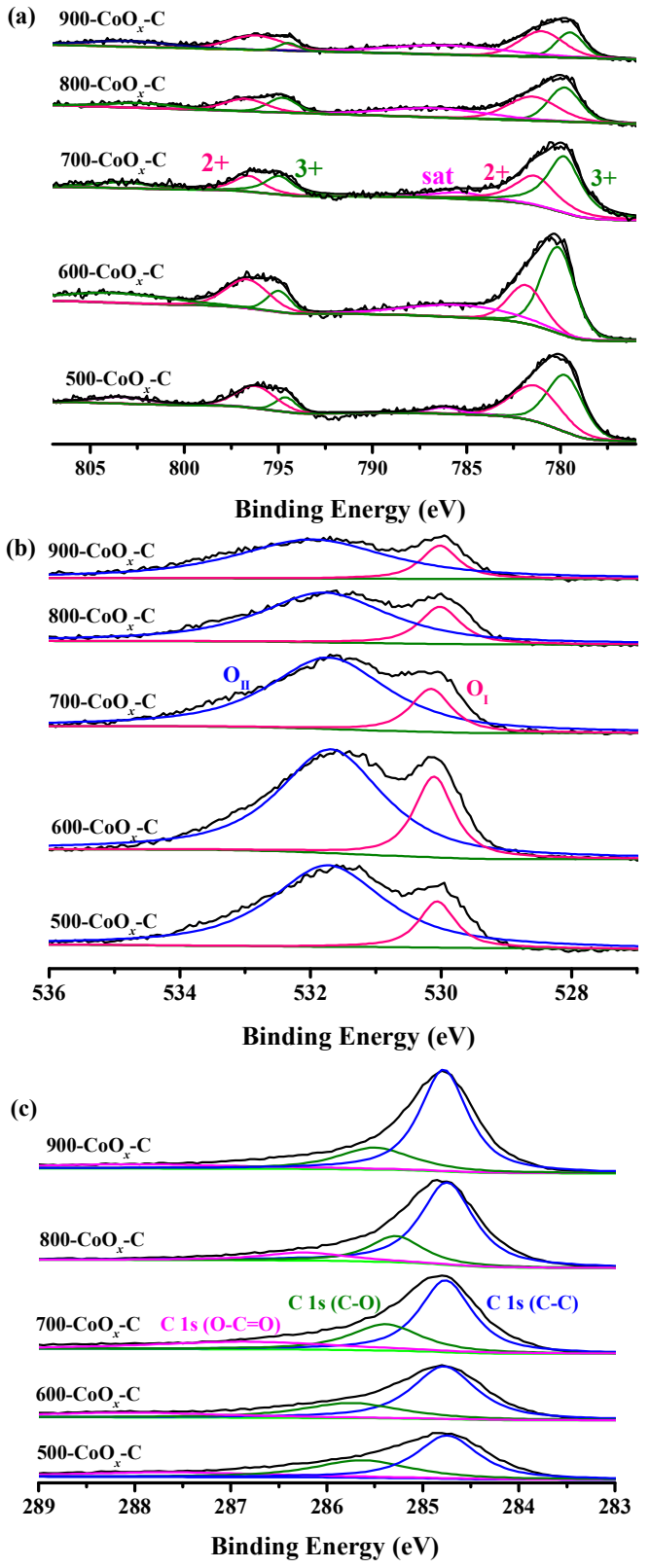

Fig 4. The XPS patterns for T-CoO_x-C.

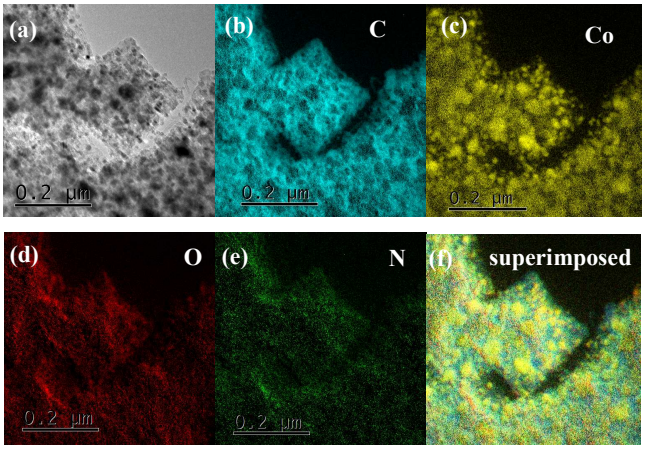

Fig 5. (a) TEM image and (b-f) EDS elemental mapping images for 700-CoO_x-C.

600-CoO_x-C, which is attributed to an insufficient carbonization temperature. The TEM images show that the CoO_x nanoparticles are homogeneously dispersed in the carbon species in sample 700-CoO_x-C (Figure S4c), whereas the CoO_x nanoparticles aggregate to form larger particles in samples 800- and 900-CoO_x-C (Figures S4d and 4e, respectively). Therefore, the homogeneity of the CoO_x nanoparticles in 800-CoO_x-C was inferior to that in 700-CoO_x-C, which was further confirmed by energy-dispersive X-ray spectroscopy (EDS) elemental mapping measurements. As shown in Figure 5, all of the elements, including C, Co, O and N, are homogeneously dispersed in 700-CoO_x-C, whereas the dispersion of Co in 700-CoO_x-C is better compared to that in 800-CoO_x-C (Figure S5). These results further demonstrate that the most suitable carbonization temperature was 700 °C, which resulted in a regular morphology and homogeneous dispersion of CoO_x in 700-CoO_x-C. Interestingly, the results of elemental analyses for T-CoO_x-C samples indicate that the Co content in 700-CoO_x-C is the lowest (Table 1), probable due to the homogeneous dispersion of CoO_x in 700-CoO_x-C. Moreover, the EDS elemental mapping images indicate that 700-CoO_x-C also contained nitrogen; nitrogen doping has been previously demonstrated to improve the catalytic efficiency of carbon-based materials via its synergistic coupling effects,[11] and N-doped graphitic carbon materials have been proven to be high-performance oxygen evolution catalysts,[11] in which the pyridinic and quaternary N atoms can act as the active sites for the OER.[11] All of these results indicate that 700 °C may be the optimal temperature for carbonization of ZIF-67 to generate the porous cobalt oxide-carbon hybrid material, 700-CoO_x-C, which was desired as a high-performance OER catalyst.

The OER catalytic activity of the resulting T-CoO_x-C hybrid materials was evaluated in a sodium borate (NaB_i) buffer solution (pH = 8.5) through a Clark oxygen electrode using $Ru(bpy)_3(PF_6)_3$ as a one electron sacrificial oxidant. Due to the high catalytic efficiency, only small scale of catalyst (0.1 ~ 1 μg, 0.3 ~ 3 μM for Co) can be added, otherwise, the amount of produced oxygen will over the solubility of saturated oxygen in solution. Usually, $[Ru(bpy)_3]^{3+}$ is *in situ* generated during photocatalytic water oxidation using $Na_2S_2O_8$ as an oxidant in combination with $[Ru(bpy)_3]^{2+}$ as a photosensitizer, in which one electron is excited by light irradiation and transformed to $S_2O_8^{2-}$ to generate a oxidized $[Ru(bpy)_3]^{3+}$ species,[5g] and many photochemical water oxidation reactions near neutral pH have used $[Ru(bpy)_3]^{2+}$-$Na_2S_2O_8$ system.[1f,4a,5g,12] However, if the rate of water oxidation catalyzed by an efficient WOC is faster than the rate of $[Ru(bpy)_3]^{3+}$ generation, $[Ru(bpy)_3]^{3+}$ generation will become a rate-determining step of overall water oxidation, in this case, the rate of water oxidation is limited by $[Ru(bpy)_3]^{3+}$ generation rather than the efficiency of WOCs. To accurately evaluate the OER catalytic activity of the T-CoO_x-C hybrid materials, we directly used a fresh prepared $Ru(bpy)_3(PF_6)_3$ as sacrificial oxidant. Though $Ru(bpy)_3(PF_6)_3$ is expensive to use as a sacrificial oxidant, the $[Ru^{III}(bpy)_3]^{3+}/[Ru^{II}(bpy)_3]^{2+}$ potential of 1.21 V *vs*. NHE is constant in the 0-14 pH range,[12a] which makes it the most appropriate oxidant to evaluate the high efficient WOCs near neutral pH, while other sacrificial oxidants such as Ce^{IV} and IO_4^- can be only used at acidic pH.[4a,12] One should keep in mind that the sacrificial oxidant was just used to evaluate the catalytic activity of WOCs, in a practical reaction system, electrons from water oxidation are used for the solar fuel production rather for the reduction of sacrificial oxidant.

As shown in Figure 6, under the same conditions, the catalytic activity of T-CoO_x-C catalysts was observed to follow the order 700-CoO_x-C > 800-CoO_x-C > 600-CoO_x-C > 900-CoO_x-C > 500-CoO_x-C, where 700-CoO_x-C exhibited the highest catalytic activity. The outstanding catalytic efficiency of 700-CoO_x-C can be attributed to the homogeneous dispersion of CoO_x nanoparticles in porous carbon generated under the optimal carbonization temperature of 700 °C, which originates from the periodic arrangement of Co(II) and imidazolate in ZIF-67. In addition, the presence of nitrogen in the hybrid material may also attribute to its outstanding catalytic efficiency, as nitrogen doping in the hybrid material has been demonstrated to be beneficial for the OER.[11] As 700-CoO_x-C exhibited the highest catalytic activity among the investigated samples, it was the only sample whose OER activity was studied in detail in the following section.

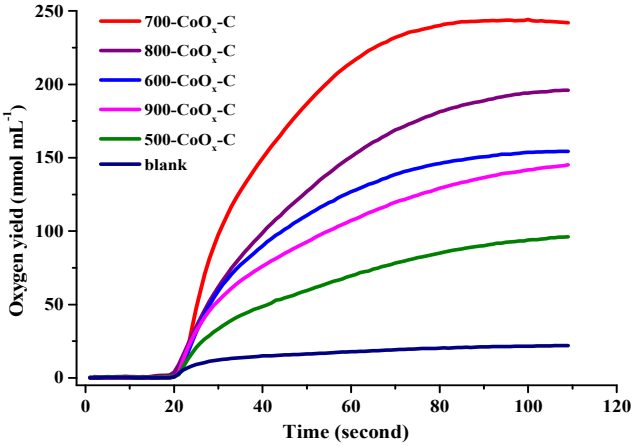

Fig 6. Oxygen yields from chemical water oxidation using $Ru(bpy)_3(PF_6)_3$ (9 mg, 4.5 mM) as an oxidant. Experimental conditions: 1 μg catalyst (3 μM for Co), 0.1 M NaB_i buffer, pH 8.5.

Water oxidation is well known to be pH-dependent; thus, the catalytic efficiency of 700-CoO_x-C was investigated under different pH conditions. As shown in Figure S6, the production of oxygen gradually increased from pH 7.0 to 8.5 because high pH values are thermodynamically favorable for water oxidation. The highest O_2 yield was detected at pH 8.5, and the yield of O_2 decreased when the pH was increased to 9.0, mainly because $Ru(bpy)_3(PF_6)_3$ is unstable at this pH.[13] Moreover, the concentration of the buffer can also affect the catalytic efficiency.[14] We therefore varied the concentration of the NaB_i buffer at pH 8.5, and a maximum yield of O_2 was observed in the case of 20 mM NaB_i buffer (Figure S7). The O_2 production decreased with increasing buffer concentration, which was caused by the faster degradation of $Ru(bpy)_3(PF_6)_3$ in the presence of higher concentrations of the buffering agent.[14] However, the amount of O_2 evolved in 10 mM NaB_i buffer was also lower than that in 20 mM NaB_i buffer because a steady pH value was difficult to maintain at this buffer concentration. Indeed, after the OER experiment, the pH of the buffer decreased from 8.5 to 7.3 when 10 mM NaB_i buffer was used, whereas the pH value remained nearly unchanged when 20 mM NaB_i buffer was used.

Under the optimized OER conditions (pH 8.5, 20 mM NaB_i buffer), the catalytic efficiency of 700-CoO_x-C was investigated using different amounts of catalyst. As shown in Figure S8 and Table S2, the TON and TOF values increased with decreasing amount of catalyst, and the maximum TON and TOF values per cobalt atom of 910 ± 21 and 14.6 ± 0.4 s^{-1}, respectively, were obtained when 0.1 μg of catalyst (0.3 μM for Co) was used. To our knowledge, such high TON and TOF values are the highest among the Co-based WOCs reported to date. Though some reports claimed that much higher TOFs of 1140 s^{-1} and 3450 s^{-1} per Co_3O_4 nanocluster were obtained,[5g, i] each Co_3O_4 nanocluster contains enormous cobalts, and the TOF per cobalt is only 0.01 s^{-1} rather than 1140 s^{-1}.[5i] It should be mentioned that the $Ru(bpy)_3(PF_6)_3$ oxidant was consumed quickly once the WOC was added to the reaction system, and the color of solution changed quickly from green ($[Ru^{III}(bpy)_3]^{3+}$) to deep orange ($[Ru^{II}(bpy)_3]^{2+}$) within 1 min, thus the decrease of oxygen generation rate along with time is attributed to the consumption of oxidant rather than the deactivation of WOC, and it is reasonable to calculate the maximum TOF based on the initial 20 s to accurately evaluate the efficiency of WOCs.[15]

To further confirm the superiority of 700-CoO_x-C as an OER catalyst, we compared its activity with those of other catalysts. For comparison, nano-Co_3O_4 was prepared through direct air-calcination of nanocrystals of ZIF-67 at 380 °C (not containing any carbon or nitrogen species, denoted as ZIF-67-Co_3O_4), which was determined by PXRD, XPS and EDS (Figures S9-10). The SEM and TEM images reveal that the obtained ZIF-67-Co_3O_4 contained relatively uniform nanoparticles (20-40 nm) (Figure S11). Water oxidation catalyzed by ZIF-67-Co_3O_4 was performed under the same conditions as those used with 700-CoO_x-C, yet ZIF-67-Co_3O_4 exhibited an inferior catalytic effect despite its higher cobalt content. Furthermore, the mixture of ZIF-67-Co_3O_4 and carbon with the same Co/C ratio as 700-CoO_x-C also resulted in poor catalysis, indicating that simple physical mixing was less effective than the strong connection between in situ formed CoO_x and carbon in 700-CoO_x-C.[5j] Notably, 700-CoO_x-C also exhibited catalytic efficiency far superior to that of commercial water-oxidation catalysts such as IrO_2 and RuO_2 (Figure 7 and Table S3). The TON value of 700-CoO_x-C was three and nine times greater than those of IrO_2 and RuO_2, respectively, and the TOF value of 700-CoO_x-C was four and fifteen times greater than those of IrO_2 and RuO_2, respectively. These results indicate that 700-CoO_x-C is indeed a highly efficient chemical WOC and could be a suitable substitute for noble-metal catalysts.

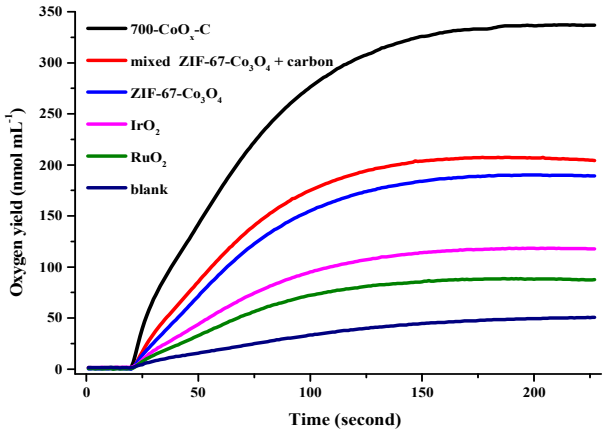

Fig 7. Oxygen yields from chemical water oxidation with $Ru(bpy)_3(PF_6)_3$ (7.5 mM) as an oxidant. Experimental conditions: 0.1 μg catalyst (0.3 μM for Co), 20 mM NaB_i buffer, pH 8.5.

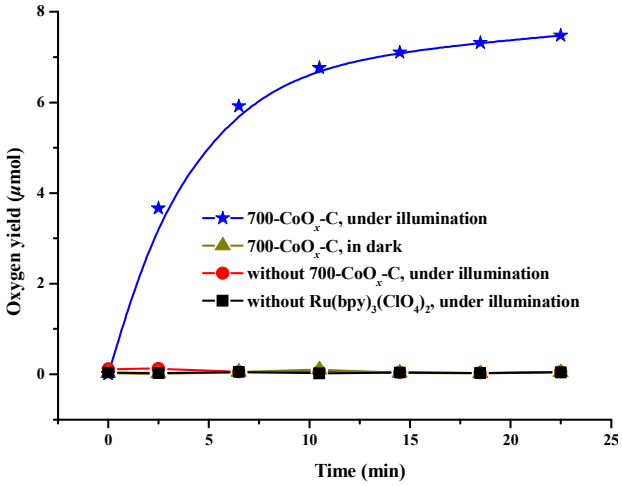

Fig 8. Time profiles of O_2 evolution in dark, under irradiation without and with 0.1 mg of 700-CoO_x-C catalyst (0.21 mM for Co), and under illumination without $[Ru(bpy)_3](ClO_4)_2$. Experimental conditions: 4.2 mM $[Ru(bpy)_3](ClO_4)_2$, 68 mM $Na_2S_2O_8$, 100 W xenon lamp ($\lambda \geq 420$ nm), 0.1 M sodium phosphate buffer with pH 8.5, total volume of solution 3.1 mL.

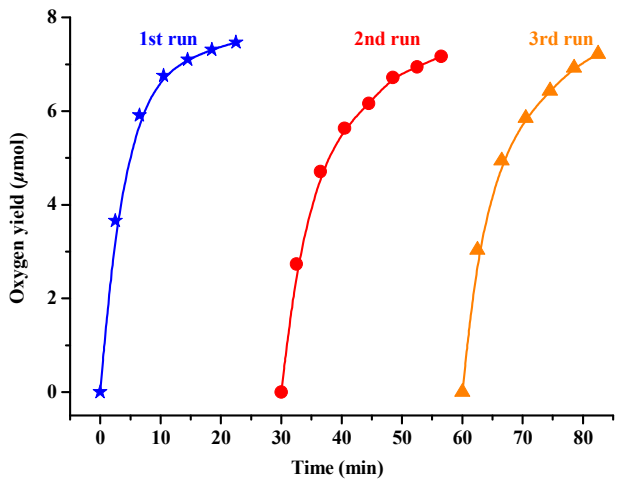

Fig 9. Time courses of O_2 evolution under photo-irradiation in three repetitive examinations at room temperature. Conditions: 0.1 mg 700-CoO_x-C (3 μM for Co), 4.2 mM $[Ru(bpy)_3](ClO_4)_2$ and 68 mM $Na_2S_2O_8$; 100 W xenon lamp ($\lambda \geq 420$ nm), 100 mM sodium phosphate buffer initial pH 8.50, total solution volume 3.1 mL.

Considering the importance of visible-light-driven catalytic water oxidation, the activity of 700-CoO_x-C was also assessed in $[Ru(bpy)_3]^{2+}$-$S_2O_8^{2-}$ system under irradiation with 100 W xenon lamp with a 420 nm cut off filter in sodium phosphate buffer (pH 8.5). The oxygen yields under different concentrations of $Na_2S_2O_8$ sacrificial electron acceptor were investigated, and giving the optimal concentrations of 22-68 mM (Figure S12). About 7.5 μmol O_2 was generated within 25 min using 10 mg (4.2 mM) of $Ru(bpy)_3(ClO_4)_2$ and 50 mg (68 mM) of $Na_2S_2O_8$ (Figure 8), the O_2 generation rate in the presence of 700-CoO_x-C is fast within initial 6 min, and then becomes slow down gradually. A maximum TOF of 0.039 ± 0.03 s^{-1} per cobalt atom is estimated. By contrast, almost no oxygen was detected under dark, or under irradiation in the absence of catalyst or $Ru(bpy)_3(ClO_4)_2$ photosensitizer (Figure 8). For comparison, recent literatures of cobalt-based OER catalysts driven by visible light have been reviewed (Supporting Information, Table S4). At present, the TOF of 0.023 s^{-1} is regarded as the highest value among all the nonprecious metal based WOCs (including Co-based WOCs) by visible light.[1f] From Table S4 it can be found that the TOF of 0.039 s^{-1} is higher than that of 0.023 s^{-1}, which is regarded as the highest value reported to date among all the nonprecious metal based water oxidation catalysts driven by visible light. Meanwhile, the TON of 12 per Co atom is also higher than those of cobalt-based OER catalysts (Table S4), further confirming the outstanding OER activity of 700-CoO_x-C under photochemical water oxidation conditions.

It is interesting to note that the above TON (12) and TOF (0.039 s^{-1}) values are much lower than the corresponding TON (910) and TOF (14.6 s^{-1}) values achieved using $Ru(bpy)_3(PF_6)_3$ directly as a one electron sacrificial oxidant. This can be attributed to the fact that the $[Ru(bpy)_3]^{3+}$ generation rate is slower than the water oxidation rate catalyzed by 700-CoO_x-C, thus $[Ru(bpy)_3]^{3+}$ generation in $[Ru(bpy)_3]^{2+}$-$S_2O_8^{2-}$ photocatalytic system is a rate-determining step of overall water oxidation, in which the rate of water oxidation is limited by $[Ru(bpy)_3]^{3+}$ generation rather than the efficiency of WOCs.[16] Thus, the TOF in photo-driven water oxidation is not the intrinsic catalytic turnover rates. To verify the rate controlling step in $[Ru(bpy)_3]^{2+}/S_2O_8^{2-}$/700-$CoO_x$-C reaction system, we monitor the accumulation of $[Ru(bpy)_3]^{3+}$ in the absence and presence of 700-CoO_x-C by UV−vis spectroscopy. As shown in Figure S13, the peaks at 453 and 670 nm are assigned to the absorption of $[Ru(bpy)_3]^{2+}$ and $[Ru(bpy)_3]^{3+}$, respectively. Clearly, UV-vis spectra show the accumulation of $[Ru(bpy)_3]^{3+}$ after 30 seconds irradiation in the absence of catalyst, while almost no $[Ru(bpy)_3]^{3+}$ was detected with the existence of 700-CoO_x-C, indicating that all the photogenerated $[Ru(bpy)_3]^{3+}$ were consumed quickly by catalyst. The above results clearly demonstrate that the generation of $[Ru(bpy)_3]^{3+}$ limits the rate of catalytic reaction, thus it is more accurate to use $[Ru(bpy)_3]^{3+}$ directly as a one electron sacrificial oxidant for evaluating the OER catalytic activity of highly efficient WOC.

The stability of 700-CoO_x-C was investigated by repetitive experiments. As shown in Figure 9, there are no significant change in the total amount of O_2 evolution in the second and third runs, indicating 700-CoO_x-C has fine activity and stability. The PXRD of 700-CoO_x-C was measured after the catalytic reaction, and its pattern is close to that of fresh catalyst (Figure S14), further demonstrating the catalyst is stable during OER.[12d,17] Thus the decrease of O_2 generation rate along with time (Figure 8) is attributed to the deactivation of photosensitizer rather than WOC.

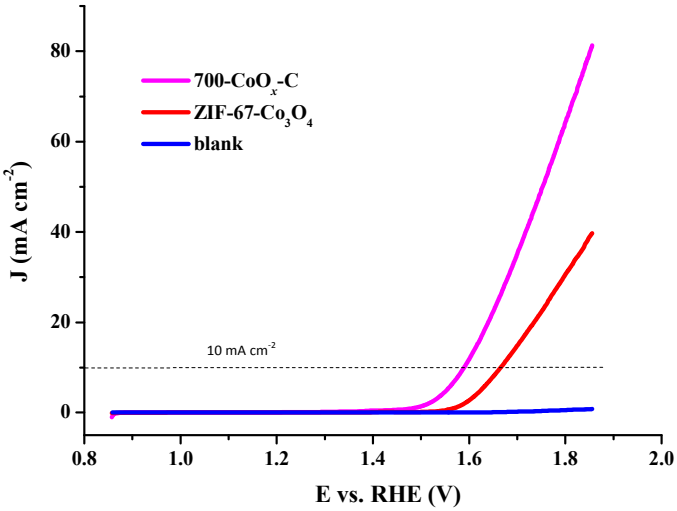

Fig 10. LSV curves for OER on bare and 700-CoO_x-C modified RDE (~0.2 mg cm^{-2}) in 0.1 M KOH solution (scan rate: 5 mV s^{-1}, 1500 rpm).

To further evaluate the water oxidation activity of 700-CoO_x-C, the electrochemical catalytic water oxidation efficiency of 700-CoO_x-C was studied by the linear sweep voltammogram (LSV). A slow scan rate (5 mV s^{-1}) was applied during the OER test on a rotating disk electrode (RDE) in alkaline solution (0.1 M KOH) to minimize the capacitive current. Potentials are reported versus the reversible hydrogen electrode (RHE). In the LSV curves (Figure 10), the bare RDE exhibits negligible catalytic activity, while the RDE modified

with 700-CoO_x-C (~0.2 mg cm^{-2}) presents notable OER current, with an OER overpotential of 0.36 V at 10.0 mA cm^{-2}, this overpotential is lower than that of 0.44 V at 10.0 mA cm^{-2} for ZIF-67-Co_3O_4 (Figure 10), and is comparable to those of the most efficient electrochemical WOCs,[5j,18] indicating 700-CoO_x-C can also act as highly efficient electrochemical WOC. The Tafel slope value of 700-CoO_x-C (89 mV dec^{-1}) is lower than that of ZIF-67-Co_3O_4 (96 mV dec^{-1}, Figure S15), suggesting the favorable reaction kinetics of 700-CoO_x-C.[5j] Moreover, the semicircular diameter in the electrochemical impedance spectrum (EIS) of 700-CoO_x-C is also lower than that of ZIF-67-Co_3O_4 (Figure S16), indicating the smaller charge transfer impedance in 700-CoO_x-C. A 4 h chronopotentiometry experiment of 700-CoO_x-C at an applied current density of 10 mA cm^2 was performed in 0.1 M KOH to probe the stability of the catalyst, and no apparent increase in potential was observed in this time frame (Figure S17), further demonstrating the good stability of the catalyst.

Conclusions

In conclusion, we reported herein a porous carbon-based hybrid with evenly distributed CoO_x nanoparticles; this material was easily synthesized by a two-step thermal treatment of cheap ZIF-67 nanocrystals. The results of SEM, TEM and EDS demonstrated that 700°C was the optimal temperature for carbonization of ZIF-67 to in situ generate the porous CoO_x-carbon hybrid material 700-CoO_x-C. This material exhibited excellent catalytic activity toward the chemical OER, with a record TOF and TON of 14.6 s^{-1} and 910, respectively. Its performance was far superior to that of commercial IrO_2 and RuO_2, as well as to those of the reported Co-based catalysts. In addition, the synthesized catalyst can also act as an efficient photochemical and electrochemical WOC, with a record TOF of 0.039 s^{-1} and an OER overpotential of 0.36 V at 10 mA cm^{-2}, respectively. The superior performance of 700-CoO_x-C was attributed to its high active surface area, homogeneous dispersion of CoO_x in porous carbon, as well as nitrogen doping. Overall, combining the superiority of highly efficient photochemical and electrochemical OER activity, easier making, and economy, 700-CoO_x-C is a promising candidate for practical use as WOCs on a large scale.

Acknowledgments

This work was supported by the 973 program of China (2012CB821706, 2014CB845602), NSFC (21331007), and NSF of Guangdong Province (S2012030006240).

Notes and references

1. (a) Y. Wu, M. Chen, Y. Han, H. Luo, X. Su, M.-T. Zhang, X. Lin, J. Sun, L. Wang, L. Deng, W. Zhang and R. Cao, *Angew. Chem. Int. Ed.*, 2015, **54**, 4870-4875; (b) Y. Zhu, W. Zhou, Z.-G. Chen, Y. Chen, C. Su, M. O. Tadé and Z. Shao, *Angew. Chem. Int. Ed.*, 2015, **54**, 3897-3901; (c) L. Duan, C. M. Araujo, M. S. G. Ahlquist and L. Sun, *PNAS*, 2012, **109**, 15584-15588; (d) M. D. Karkas, T. Akermark, H. Chen, J. Sun and B. Akermark, *Angew. Chem. Int. Ed.*, 2013, **52**, 4189-4193; (e) J. L. Fillol, Z. Codolà, I. Garcia-Bosch, L. Gómez, J. J. Pla and M. Costas, *Nat. Chem.*, 2011, **3**, 807-813; (f) G. S. Hutchings, Y. Zhang, J. Li, B. T. Yonemoto, X. Zhou, K. Zhu and F. Jiao, *J. Am. Chem. Soc.*, 2015, **137**, 4223-4229; (g) Y. Jiang, F. Li, B. Zhang, X. Li, X. Wang, F. Huang and L. Sun, *Angew. Chem. Int. Ed.*, 2013, **52**, 3398-3401; (h) L. Duan, F. Bozoglian, S. Mandal, B. Stewart, T. Privalov, A. Llobet and L. Sun, *Nat. Chem.*, 2012, **4**, 418-423.

2. (a) E. A. Paoli, F. Masini, R. Frydendal, D. Deiana, C. Schlaup, M. Malizia, T. W. Hansen, S. Horch, I. E. L. Stephens and I. Chorkendorff, *Chem. Sci.*, 2015, **6**, 190-196; (b) R. D. L. Smith, B. Sporinova, R. D. Fagan, S. Trudel and C. P. Berlinguette, *Chem. Mater.*, 2014, **26**, 1654-1659; (c) N. Danilovic, R. Subbaraman, K. C. Chang, S. H. Chang, Y. Kang, J. Snyder, A. P. Paulikas, D. Strmcnik, Y. T. Kim, D. Myers, V. R. Stamenkovic and N. M. Markovic, *Angew. Chem. Int. Ed.*, 2014, **53**, 14016-14021; (d) X. Long, J. Li, S. Xiao, K. Yan, Z. Wang, H. Chen and S. Yang, *Angew. Chem. Int. Ed.*, 2014, **53**, 7584-7588.

3. K. S. Joya, Y. F. Joya, K. Ocakoglu and R. van de Krol, *Angew. Chem. Int. Ed.*, 2013, **52**, 10426-10437.

4. (a) T. Takashima, k. Hashimoto and R. Nakamura, *J. Am. Chem. Soc.*, 2012, **134**, 18153-18156; (b) D. M. Robinson, Y. B. Go, M. Mui, G. Gardner, Z. Zhang, D. Mastrogiovanni, E. Garfunkel, J. Li; M. Greenblatt and G. C. Dismukes, *J. Am. Chem. Soc.*, 2013, **135**, 3494-3501; (c) A. Indra, P. W. Menezes, I. Zaharieva, E. Baktash, J. Pfrommer, M. Schwarze, H. Dau and M. Driess, *Angew. Chem. Int. Ed.*, 2013, **52**, 13206-13210; (d) M. M. Najafpour, A. N. Moghaddam, H. Dau and I. Zaharieva, *J. Am. Chem. Soc.*, 2014, **136**, 7245-7248; (e) Y, Meng, W. Song, H. Huang, Z. Ren, S.-Y. Chen and S. L. Suib, *J. Am. Chem. Soc.*, 2014, **136**, 11452-11464; (f) R. Pokhrel, M. K. Goetz, S. E. Shaner, X. Wu and S. S. Stahl, *J. Am. Chem. Soc.*, 2015, **137**, 8384-8387; (g) J. Wang, K. Li, H.-X. Zhong, D. Xu; Z.-L. Wang, Z.-J. Wu and X.-B. Zhang, *Angew. Chem. Int. Ed.*, 2015, **54**, 10530-10534; (h) H. Wang, H.-W. Lee, Y. Deng, Z. Lu, P.-C. Hsu, Y. Liu, D. Lin and Y. Cui, *Nat. Commun.*, 2015, **6**, 7261; (i) L. Kuai, J. Geng, C. Chen, E. Kan, Y. Liu, Q. Wang and B. Geng, *Angew. Chem. Int. Ed.*, 2014, **53**, 7547-7551; (j) M. Gao, W. Sheng, Z. Zhuang, Q. Fang, S. Gu, J. Jiang and Y. Yan, *J. Am. Chem. Soc.*, 2014, **136**, 7077-7084; (k) C.-H. Kuo, W. Li, L. Pahalagedara, A. M. El-Sawy, D. Kriz, N. Genz, C. Guild, T. Ressler, S. L. Suib and J. He, *Angew. Chem. Int. Ed.*, 2015, **54**, 2345-2350; (l) B. Iandolo and A. Hellman, *Angew. Chem. Int. Ed.*, 2014, **53**, 13404-13408; (m) G. Chen, L. Chen, S.-M. Ng, W.-L. Man and T.-C. Lau, *Angew. Chem. Int. Ed.*, 2013, **52**, 1789-1791; (n) Y.-F. Li and A. Selloni, *ACS Catal.*, 2014, **4**, 1148-1153; (o) M. Gao, W. Sheng, Z. Zhuang, Q. Fang, S. Gu, J. Jiang and Y. Yan, *J. Am. Chem. Soc.*, 2014, **136**, 7077-7084.

5. (a) S. Chen, S. Shen, G. Liu, Y. Qi, F. Zhang and C. Li, *Angew. Chem. Int. Ed.*, 2015, **54**, 3047-3051; (b) M. W. Kanan and D. G. Nocera, *Science*, 2008, **321**, 1072-1075; (c) W. Chaikittisilp, N. L. Torad, C. Li, M. Imura, N. Suzuki, S. Ishihara, K. Ariga and Y. Yamauchi, *Chem. Eur. J.*, 2014, **20**, 4217-4221; (d) G. P. Gardner, Y. B. Go, D. M. Robinson, P. F. Smith, J. Hadermann, A. Abakumov, M. Greenblatt and G. C. Dismukes, *Angew. Chem. Int. Ed.*, 2012, **51**, 1616-1619; (e) F. Song and X. Hu, *Nat. Commun.*, 2014, **5**, 4477; (f) Z. Zhuang, W. Sheng and Y. Yan, *Adv. Mater.*, 2014, **26**, 3950-3955; (g) X. Deng and H. Tüysüz, *ACS Catal.*, 2014, **4**, 3701-3714; (h) J. D. Blakemore, H. B. Gray, J. R. Winkler and A. M. Müller, *ACS Catal.*, 2013, **3**, 2497-2500; (i) F. Jiao and H. Frei, *Angew. Chem. Int. Ed.*, 2009, **48**, 1841-1844; (j) T. Y. Ma, S. Dai, M. Jaroniec and S. Z. Qiao, *J. Am. Chem. Soc.*, 2014, **136**, 13925-13931; (k) S. Yusuf and F. Jiao, *ACS Catal.*, 2012, **2**, 2753-2760; (l) A. J. Esswein, M. J. McMurdo, P. N. Ross, A. T. Bell and T. D. Tilley, *J. Phys. Chem. C*, 2009, **113**, 15068-15072; (m) C.-C. Lin, Y. Guo and J. Vela, *ACS Catal.*, 2014, **5**, 1037-1044; (n) J. Rosen, G. S. Hutchings and F. Jiao, *J. Am. Chem. Soc.*, 2013, **135**, 4516-4521; (o) M. Zhang, M. de Respinis and H. Frei, *Nat. Chem.*, 2014, **6**, 362-367; (p) J. Huang, J, Chen, T. Yao, J. He, S. Jiang, Z. Sun, Q. Liu, W. Cheng, F. Hu, Y. Jiang, Z. Pan and S. Wei, *Angew. Chem. Int. Ed.*, 2015, **54**, 8722-8727.

6. (a) Z. Wang, X. Li, H. Xu, Y. Yang, Y. Cui, H. Pan, Z. Wang, B. Chen and G. Qian, *J. Mater. Chem. A*, 2014, **2**, 12571-12575; (b) S. Ma, G. A. Goenaga, A. V. Call and D.-J. Liu, *Chem. Eur. J.*, 2011, **17**, 2063-2067; (c) Z. Wang, X. Li, Y. Yang, Y. Cui, H. Pan, Z. Wang, B. Chen and G. Qian, *J. Mater. Chem. A*, 2014, **2**, 7912-7916; (d) H. L. Jiang, B. Liu, Y. Q. Lan, K. Kuratani, T. Akita, H. Shioyama, F. Zong and Q. Xu, *J. Am. Chem. Soc.*, 2011, **133**, 11854-11857.

7. R. Banerjee, A. Phan, B. Wang, C. Knobler, H. Furukawa, M. O'Keeffe and O. M. Yaghi, *Science*, 2008, **319**, 939-943.

8. (a) W. Xia, J. Zhu, W. Guo, L. An, D. Xia and R. Zou, *J. Mater. Chem. A*, 2014, **2**, 11606-11613; (b) Y. Hou, Z. Wen, S. Cui, S. Ci, S. Mao and J.

Chen, *Adv. Funct. Mater.*, 2015, **25**, 872-882; (c) X. Wang, J. Zhou, H. Fu, W. Li, X. Fan, G. Xin, J. Zheng and X. Li, *J. Mater. Chem. A*, 2014, **2**, 14064-14070; (d) Y.-Z. Chen, C. Wang, Z.-Y, Wu, Y, Xiong, Q. Xu, S.-H. Yu and H.-L. Jiang, *Adv. Mater.*, 2015, **27**, 5010-5016. (e) L. Zhang, W. He, X. Xiang, Y. Li and F. Li, *RSC Adv.*, 2014, **4**, 43357-43365. (f) Z.-S. Wu, W. Ren, L. Wen, L. Gao, J. Zhao, Z. Chen, G. Zhou, F. Li and H.-M. Cheng, *ACS Nano*, 2010, **4**, 3187-3194.

9. Z. Jiang, Z. Li, Z. Qin, H. Sun, X. Jiao and D. Chen, *Nanoscale*, 2013, **5**, 11770-11775.
10. (a) H. N. Nong, H.-S. Oh, T. Reier, E. Willinger, M.-G. Willinger, V. Petkov, D. Teschner and P. Strasser, *Angew. Chem. Int. Ed.*, 2015, **54**, 2975-2979; (b) B. Liu, C.-H. Kuo, J. Chen, Z. Luo, S. Thanneeru, W. Li, W. Song, S. Biswas, S. L. Suib and J. He, *Angew. Chem. Int. Ed.*, 2015, **54**, 9061-9065; (c) F. Liang, C. Wu, H. Lin, T. Li, D. Gao, Z. Li, J. Wei, C. Zheng and M. Sun, *Bioorg. Med. Chem. Lett.*, 2003, **13**, 2469-2472.
11. (a) S. Chen, J. Duan, M. Jaroniec and S.-Z. Qiao, *Adv. Mater.*, 2014, **26**, 2925-2930; (b) Y. Zhao, R. Nakamura, K. Kamiya, S. Nakanishi and K. Hashimoto, *Nat. Commun.*, 2013, **4**, 2390-2396; (c) T. Y. Ma, S. Dai, M. Jaroniec and S. Z. Qiao, *Angew. Chem. Int. Ed.*, 2014, **53**, 7281-7285; (d) K. Gong, F. Du, Z. Xia, M. Durstock, L. Dai, *Science*, 2009, **323**, 760-764.
12. (a) A. R. Parent, R. H. Crabtree and G. W. Brudvig, *Chem. Soc. Rev.*, 2013, **42**, 2247-2252; (b) M. Yoshida, M. Kondo, S. Torii, K. Sakai and S. Masaoka, *Angew. Chem. Int. Ed.*, 2015, **54**, 7981-7984; (c) L. Ma, Q. Wang, W.-L. Man, H.-K. Kwong, C.-C. Ko and T.-C. Lau, *Angew. Chem. Int. Ed.*, 2015, **54**, 5246-5249; (d) Y. Yamada, K. Oyama, R. Gates and S. Fukuzumi, *Angew. Chem. Int. Ed.*, 2015, **54**, 5613-5617.
13. G. Chen, L. Chen, S. M. Ng and T. C. Lau, *ChemSusChem*, 2014, **7**, 127-134.
14. F. Song, Y. Ding, B. Ma, C. Wang, Q. Wang, X. Du, S. Fu and J. Song, *Energy Environ. Sci.*, 2013, **6**, 1170-1184.
15. (a) M. D. Kärkäs, T. Åkermark, E. V. Johnston, S. R. Karim, T. M. Laine, B.-L. Lee, T. Åkermark, T. Privalov and B. Åkermark, *Angew. Chem. Int. Ed.*, 2012, **51**, 11589-11593; (b) H. Lv, J. Song, Y. V. Geletii, J. W. Vickers, J. M. Sumliner, D. G. Musaev, P. Kogerler, P. F. Zhuk, J. Bacsa, G. Zhu and C. L. Hill, *J. Am. Chem. Soc.*, 2014, **136**, 9268-9271.
16. Y. V. Geletii, Z. Huang, Y. Hou, D. G. Musaev, T. Lian and C. L. Hill, *J. Am. Chem. Soc.*, 2009, **131**, 7522-7523.
17. D. Hong, Y. Yamada, T. Nagatomi, Y. Takai and S. Fukuzumi, *J. Am. Chem. Soc.*, 2012, **134**, 19572-19575.
18. Y. Liu, H. Cheng, M. Lyu, S. Fan, Q. Liu, W. Zhang, Y. Zhi, C. Wang, C. Xiao, S. Wei, B. Ye and Y. Xie, *J. Am. Chem. Soc.*, 2014, **136**, 15670-15675.

TOC graphic for

A facile method for the synthesis of a porous cobalt oxide-carbon hybrid as a highly efficient water oxidation catalyst

Mei Zhang, Yong-Liang Huang, Jia-Wei Wang and Tong-Bu Lu*

A cobalt oxide-carbon hybrid was synthesized, which exhibited outstanding chemical, photochemical and electrochemical water oxidation catalytic activity.